ADVANCED FUNCTIONAL MATERIALS

www.afm-journal.de

# In Vivo Self-Powered Wireless Transmission Using Biocompatible Flexible Energy Harvesters

*Dong Hyun Kim, Hong Ju Shin, Hyunseung Lee, Chang Kyu Jeong, Hyewon Park, Geon-Tae Hwang, Ho-Yong Lee, Daniel J. Joe, Jae Hyun Han, Seung Hyun Lee, Jaeha Kim,* Boyoung Joung,* and Keon Jae Lee**

**Additional surgeries for implantable biomedical devices are inevitable to replace discharged batteries, but repeated surgeries can be a risk to patients, causing bleeding, inflammation, and infection. Therefore, developing self-powered implantable devices is essential to reduce the patient's physical/psychological pain and financial burden. Although wireless communication plays a critical role in implantable biomedical devices that contain the function of data transmitting, it has never been integrated with in vivo piezoelectric self-powered system due to its high-level power consumption (microwatt-scale). Here, wireless communication, which is essential for a ubiquitous healthcare system, is successfully driven with in vivo energy harvesting enabled by high-performance single-crystalline $(1-x)Pb(Mg_{1/3}Nb_{2/3})O_3$–$(x)Pb(Zr,Ti)O_3$ (PMN-PZT). The PMN-PZT energy harvester generates an open-circuit voltage of 17.8 V and a short-circuit current of 1.74 μA from porcine heartbeats, which are greater by a factor of 4.45 and 17.5 than those of previously reported in vivo piezoelectric energy harvesting. The energy harvester exhibits excellent biocompatibility, which implies the possibility for applying the device to biomedical applications.**

## 1. Introduction

The prevalence rates of chronic diseases have risen along with aging of the global population, which strongly calls for ubiquitous healthcare (u-Health) systems for in situ monitoring and diagnoses.[1,2] Implantable biomedical devices used for u-Health systems contain the function of vital sign sensing as well as data transmitting.[3,4] However, wireless communication for data transmission significantly increases power consumption, which in turn decreases the battery lifetime.[5,6] Thus, repeated and additional surgeries are inevitable to replace discharged batteries every five to eight years due to the limited battery life of implantable medical devices.[7] However, battery-replacement surgery can cause inflammation, bleeding, and infection, and induce detrimental outcomes, especially for the elderly patients who are vulnerable to complications and side effects.[8] Therefore, developing sustainable self-powered implantable electronics is necessary to reduce the patient's physical, psychological, and financial burden. Although several researchers have explored various power supplies for medical electronic implants, such as wireless charging technologies[9–12] and implanted photovoltaic devices,[13] they have critical drawbacks resulting from

D. H. Kim, Dr. D. J. Joe, J. H. Han, S. H. Lee, Prof. K. J. Lee
Department of Materials Science and Engineering
Korea Advanced Institute of Science and Technology (KAIST)
291 Daehak-ro, Yuseong-gu, Daejeon 34141, Republic of Korea
E-mail: keonlee@kaist.ac.kr

Prof. H. J. Shin[+]
Department of Thoracic and Cardiovascular Surgery
Chungbuk National University Hospital
College of Medicine
Chungbuk National University
1 Chungdae-ro, Seowon-gu, Cheongju
Chungcheongbuk-do 28644, Republic of Korea

H. Lee, Prof. J. Kim
Department of Electrical Engineering and Computer Science
Seoul National University
1 Gwanak-ro, Gwanak-gu, Seoul 08826, Republic of Korea
E-mail: jaeha@snu.ac.kr

Dr. C. K. Jeong
KAIST Institute for NanoCentury (KINC)
291 Daehak-ro, Yuseong-gu, Daejeon 34141, Republic of Korea

H. Park, Prof. B. Joung
Division of Cardiology
Severance Cardiovascular Hospital
Yonsei University Health System
Yonsei University College of Medicine
50 Yonsei-ro, Seodaemun-gu, Seoul 03722, Republic of Korea
E-mail: cby6908@yuhs.ac

Dr. G.-T. Hwang
Functional Ceramic Group
Korea Institute of Materials Science (KIMS)
797 Changwon-daero, Seongsan-gu, Changwon
Gyeongsangnam-do 51508, Republic of Korea

Dr. H.-Y. Lee
Ceracomp Co., Ltd.
42 Baekseokgongdan 1-ro, Seobuk-gu, Cheonan-si
Chungcheongnam-do 31094, Republic of Korea

[+]Present address: Department of Thoracic and Cardiovascular Surgery, Korea University Ansan Hospital, Korea University College of Medicine, 123 Jeokgeum-ro, Danwon-gu, Ansan-si, Gyeonggi-do 15355, Republic of Korea

**DOI: 10.1002/adfm.201700341**

 

electromagnetic damage and low energy efficiency in human body, respectively.

A feasible alternative is converting biomechanical energy into electrical energy to power implantable biomedical devices because there are abundant mechanical movements of internal organs such as hearts, lungs, and diaphragms.[14,15] Triboelectric energy harvesters have recently been attempted to achieve biomechanical energy harvesting,[16–18] but they have intrinsic limitations such as susceptibility to humidity, stability, and surface damage from friction.[19] In contrast, flexible piezoelectric energy harvesters have attracted much attentions as a self-powered energy source due to its high flexibility and robust stability in the confined living body.[20–27] As flexible piezoelectric materials, several researchers have investigated PZT ribbons[28] and polyvinylidene difluoride (PVDF) films[29] to harvest energy from the continuous motion of the circulatory system. They reported current levels of a few hundreds of nA generated by regular heartbeats, but the output power was too low to operate practical electronic applications due to insufficient material properties.

Recently, our group has demonstrated highly efficient flexible piezoelectric energy harvesters using single crystals for biomedical application.[30–34] However, the above papers demonstrated the operation of medical devices using in vitro harvested energy from the bending stage. Thus, to realize in vivo self-powered systems, there are still critical issues to be investigated, including large animal model experiments, biocompatibility tests, and practical device operation such as wireless communication, sensing, and pacing. In particular, a large animal model is necessary to prove the practical use of an energy harvester in the human body before human clinical trials. It is also essential to check biocompatibility of the single-crystalline generator to avoid producing an adverse effect like necrosis or inflammation. In addition, wireless communication devices should operate with in vivo energy harvesting to establish fully self-powered implantable u-Health systems. Although the concept of wireless data transmission using in vivo energy harvesting has been recently suggested by several researchers, these systems have never been integrated with in vivo piezoelectric energy harvesters due to the requirement of microwatt-scale power consumption.[35–37]

In this study, we demonstrate the self-powered wireless data transmission enabled by harvesting in vivo biomechanical energy with a high-performance piezoelectric energy harvester in a large animal model. From the contraction and relaxation of a porcine heart, the single-crystalline flexible energy harvester generated a short-circuit current of 1.75 μA (open-circuit voltage of 17.8 V), which is higher by a factor of 17.5 than that of previously reported in vivo piezoelectric energy harvesting.[28] Various cell viability tests and the histological aspects were also performed to show the biocompatibility of a flexible single-crystalline generator, which revealed no serious sign of cytotoxic damage and inflammatory reaction. Finally, we were able to wirelessly transmit communication data using the self-powered system driven by the porcine heartbeat. It was also visually proved by repeatedly switching on and off a light bulb at a long distance of about 5 m without any other power source. This successful self-powered wireless data transmission shows the possibility of powerful application to u-Health systems directly using biomechanical energy harvesting.

## 2. Results and Discussion

**Figure 1**a illustrates the conceptual scheme for in vivo self-powered system using a flexible single-crystalline $(1-x)Pb(Mg_{1/3}Nb_{2/3})O_3$–$(x)Pb(Zr,Ti)O_3$ with 0.5 mol% Mn doping (PMN-PZT-Mn) energy harvester attached to a porcine heart. The Mn-doped PMN-PZT crystal has high piezoelectric charge coefficient ($d_{33} \approx 1140$ pC $N^{-1}$)[38,39] and electromechanical coupling factor ($k_{33} \approx 0.92$), which is significantly greater than other PZT materials.[38] The figure of merit of PMN-PZT-Mn, an important factor for evaluating piezoelectric property, was found to be one order of magnitude higher than that of undoped PMN-PZT because of the high mechanical quality factor (Table S1, Supporting Information). Moreover, the third-generation single-crystalline PMN-PZT-Mn exhibited negligible dependence on the thickness due to higher coercive and internal bias field,[38] which can be a great advantage for flexible energy harvesters that require thin film for flexibility. The flexible energy harvester was fabricated by a protocol similar to our previous report[32] as shown in the Experimental Section. To simulate the feasibility of energy harvesting in a human body, a large animal model was set up in an adult pig, which has a heart anatomy similar to that of human beings.[40] Wireless data transmission as a practical application was carried out with the energy derived from periodic porcine heartbeats. Figure 1b shows that the flexible PMN-PZT-Mn harvester bent by human fingers has high mechanical flexibility and durability during bending deformation. As shown in the scanning electron microscopy (SEM) image of the PMN-PZT-Mn thin film

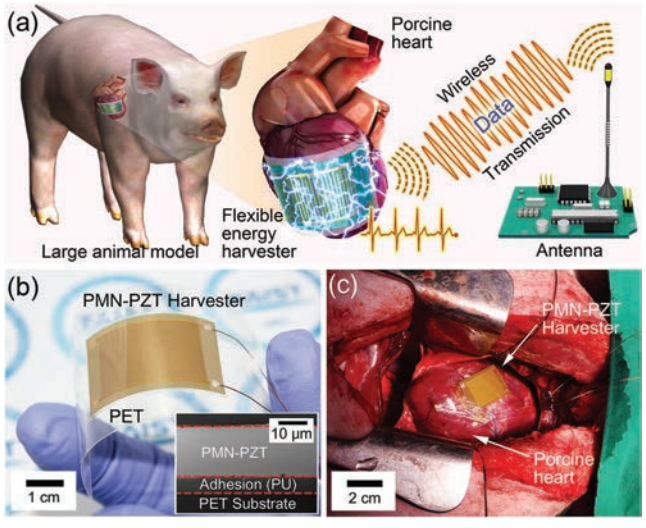


**Figure 1.** a) Conceptual scheme for the in vivo self-powered system. The flexible energy harvester attached to a porcine heart generated electricity from rhythmical cardiac contraction and relaxation. Energy derived from the heart can be used in wireless data transmission which is essential to the u-Health system. b) The flexible energy harvester bent by human fingers. The inset is an SEM image of the single-crystalline PMN-PZT-Mn thin film on the PET substrate. c) A photograph of the device affixed to a porcine heart between the right ventricle and left ventricular apex.

on the polyethylene terephthalate (PET) substrate (inset of Figure 1b), the single crystal was successfully transferred on a plastic substrate without any waviness, fracture, or crack. Excellent crystallinity of the PMN-PZT-Mn thin film after the transfer process was clearly observed through an X-ray diffraction analysis (Figure S1, Supporting Information), a transmission electron microscopy (TEM), and a selected area electron diffraction pattern (Figure S2, Supporting Information). This superior crystallinity of the flexible single crystal piezoelectric thin film produced an outstanding output of the energy harvester.

The flexible energy harvester was implanted in a porcine heart, as presented in Figure 1c. An adult Yorkshire pig (male, 40 kg) was anesthetized, and then endotracheal intubation in the pig was performed for mechanical ventilation. After a median sternotomy, the energy harvester was sutured onto the epicardium with one stitch at each corner of the device to maintain conformal contact. A flexible piezoelectric energy harvester based on a polymer film (75 μm thickness) has bending stiffness of $9.95 \times 10^{-5}$ Nm, smaller than that of medical patch for cardiac surgery ($2.52 \times 10^{-3}$ Nm), which would not affect the physiological activity of the heart.[40] Among various locations, the strongest flexion of the device was achieved when the device was fixed at the region between right ventricle and left ventricular apex.[40] It is notable that the flexible energy harvester was smoothly deformed with slight displacement even in a vigorous contraction of ventricles (Video S1, Supporting Information), which provided high stability and durability during contraction and relaxation motions of the heart.

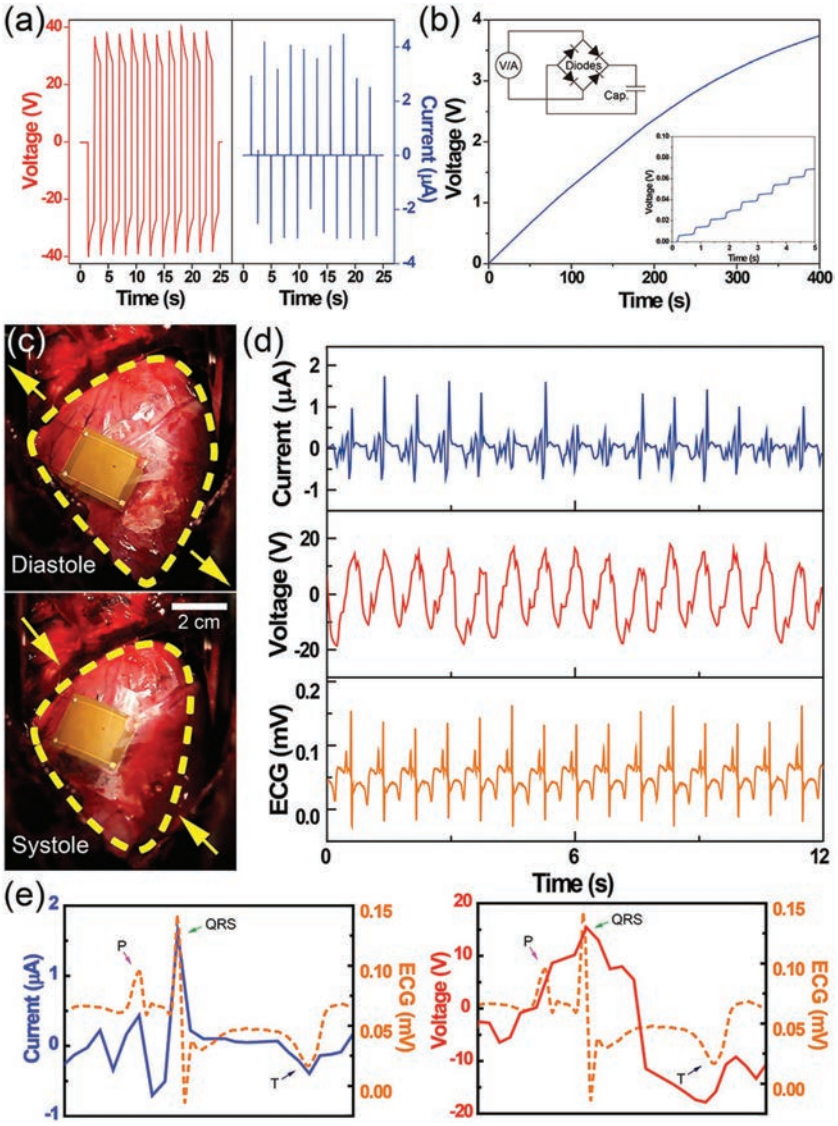


**Figure 2.** a) The generated output open-circuit voltage and short-circuit current from the flexible energy harvester during the periodical bending and unbending motions on a linear stage. b) The charged voltage in a 22 μF capacitor with the flexible energy harvester. The upper inset presents a schematic circuit diagram. The lower inset is a magnified view of the charging graph in time scale from 0 to 5 s. c) Photographs of the device when the heart relaxes in diastole (top) and contracts in systole (bottom). d) In vivo output open-circuit voltage and short-circuit current of the device derived from porcine heartbeat and simultaneously recorded ECG signals of the pig. e) Magnified view of the ECG, current, and voltage peak.

**Figure 2**a shows the electrical output performance of the flexible PMN-PZT-Mn energy harvester through mechanical bending and unbending deformations on a linear stage. The harvesting device generated an open-circuit voltage of 40 V and a short-circuit current of 4.5 μA with a curvature radius of 2 cm and a frequency of 0.4 Hz. As shown in Figure S3 in the Supporting Information, the flexible energy harvester could respond to various frequencies (1.7, 2.7, 5.3 Hz). Performance stability is important to operate the device for a long time. A bending fatigue test was performed to verify long-term stability and durability of flexible energy harvester. The output voltage signals were steadily observed without performance degradation during around 100 000 bending and releasing cycles as shown in Figure S4 in the Supporting Information. Note that bending curvature in actual in vivo conditions (κ: 0.17 $cm^{-1}$) such as the heart and diaphragm is much less than that of our fatigue test (κ: 0.50 $cm^{-1}$), which definitely increases performance stability. Figure 2b presents the charging curve of a 22 μF capacitor from 0 to 3.7 V for 400 s using the flexible PMN-PZT-Mn energy harvester with 1 Hz continual bending and unbending deformation. The electrical output was rectified to charge a capacitor with a full-wave bridge rectifier of which the circuit diagram is displayed in the upper inset of Figure 2b. In full-wave bridge rectifier, the four diodes are arranged in series pairs with only two diodes, which makes the current flowing through the capacitor unidirectional (Figure S5, Supporting Information). The lower inset is a magnified view of the charging graph,

which indicates a step curve by each cycle of bending and unbending of the flexible generator.

Figure 2c shows that the energy harvesting device fixed on the epicardium bent and released when the heart contracted in the systole and relaxed in the diastole, respectively. Two powerful beats appeared in a cycle of the heartbeat, corresponding to the atrial and ventricular systole. The ventricular systole produced a large deformation of the flexible piezoelectric film because of its stronger contractility than that of the atria. From the contraction and relaxation motion of the porcine heart, the flexible energy harvester generated an open-circuit voltage of 17.8 V and a short-circuit current of 1.75 μA (Figure 2d), which were higher by a factor of 4.45 and 17.5 than that of previously reported in vivo piezoelectric energy harvesting.[28] Note that the output current has been significantly improved compared to the previous research. This high level output current is extremely important for practical application such as wireless communication, sensing, and pacing. Especially, generating at least a microampere level of current is crucial for wireless communication that has a power consumption of several microwatts and driving voltage of a few volts.[35] These outstanding performances were obtained because of the remarkable piezoelectric charge coefficient as well as the minimal-thickness dependence of the third-generation single crystals.

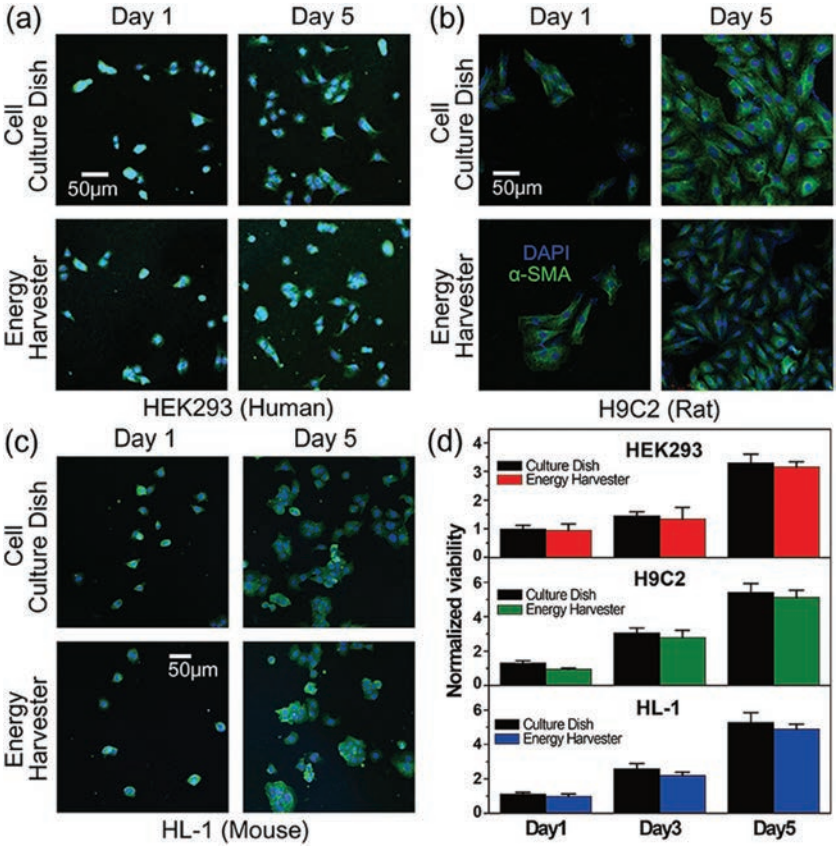


**Figure 3.** Immunofluorescence images of stained a) HEK293 cells, b) H9C2, and c) HL-1, which were cultured on a cell culture dish and flexible energy harvester. The panels show the cells grown on the culture dish after a day (left upper panel), on the device after a day (left lower panel), on the culture dish after 5 days (right upper panel), and on the device after 5 days (right lower panel). d) Normalized viability of three kinds of cells after being cultured for 5 days.

The electrical output signals generated from the flexible energy harvester were well synchronized with electrocardiogram (ECG) signals from the porcine heart, as shown in Figure 2d, which proves that the generated electricity was originally derived from cardiac motions. Due to its accurate coincidence with ECG signals, the energy harvester could be applied to a heart monitoring sensor, detecting cardiac information such as normal and abnormal heart rates. For example, the normal heart rate of the pig was 75.9 BPM, which was easily calculated as the peak-to-peak interval of electrical signals of 0.79 s (Supporting Information). To compare output signals with ECG signals in detail, each ECG, current, and voltage peak is magnified in Figure 2e. A normal ECG comprises several characteristic waves that arise from the electrical conduction system of the heart.[41] The first upright wave called the P wave corresponds to atrial depolarization, which causes the myocardium of the atria to contract. The QRS complex represents ventricular depolarization that results in the contraction of the left and right ventricles. The T wave, the last event of the cycle, indicates repolarization of the ventricles, which restores the resting state. All the characteristic waves (P, QRS, and T waves) were clearly revealed in the output current signals as expressed in the left panel of Figure 2e, although there was a subsidiary wave around the P wave. This residual minor signal was presumably due to some mechanical deviations, such as the cardiac oscillation resulting from turbulent blood flow, the pulsation of coronary arteries on the surface of the heart, and the nonsynchronous contraction of other parts of the heart, etc.[18] While the generated output voltage signal has a little different waveform from the ECG signal due to the capacitance of the device and source-meter, the change of the detailed value by each characteristic wave was obviously manifested, as shown in the right panel of Figure 2e.

Biomedical applications inside living bodies require the reliable evaluation of biocompatibility to prevent adverse influences on surrounding tissues. As shown in **Figure 3**, to study the effect of the single-crystalline generator on the body, a cytotoxicity test was carried out via a comparison of the cell viability. Three different species were chosen as common tissue cell lines: human embryonic kidney cells (HEK293), rat cardiomyoblasts (H9C2), and the mouse cardiac muscle cell line (HL-1). Cells of the control group were grown on the general cell culture dish, and then the same species cells were also incubated on the device for the experimental group. The incubated cells were stained with alpha smooth muscle actin (α-SMA) and 4′,6-diamidino-2-phenylindole (DAPI) for taking fluorescence images with a confocal microscope. The myofibroblast formation was marked in green with α-SMA and nuclei were stained blue with DAPI. Figure 3a–c shows immunofluorescence

images of HEK293, H9C2, and HL-1, respectively. Images display cells were grown on the culture dish after a day (left upper panel), on the device after a day (left lower panel), on the culture dish after 5 days (right upper panel), and on the device after 5 days (right lower panel). The images after 3 days of culture are also shown in Figure S6 in the Supporting Information. Live cells with undamaged nuclei were clearly shown during all periods of the culture, which means that all kinds of cells were readily spread with intact cytoarchitecture for both the control and experimental groups. Viability of the control group showed no significant differences from that of the experimental group as shown in Figure 3d. Note that PMN-PZT-Mn energy harvester had no detectable cytotoxicity to diverse species including human beings. Although the piezoelectric layer contains Pb, PZT-based materials are known to be nontoxic to cells in the crystalline state.[42] Moreover, the third-generation single crystals lead to a substantial increase in crystal stability,[43,44] which reduces chemical reactivity with surrounding cells. Little toxicity is further enhanced by complete encapsulation with biocompatible passivation epoxy (SU-8).[45,46] The SU-8 passivation layer also prevents the generated electricity from affecting the physiological activity of porcine heart due to its excellent electrical insulation.[47–49]

In addition to cellular toxicity, we also tested inflammatory reactions against the device to consider histological effects of the implanting situation. The PMN-PZT-Mn flexible energy harvester with a size of 1 cm × 1 cm was inserted under the dorsal skin of normal rats. After some given implantation periods, the dorsal tissue was transversely sliced and stained with hematoxylin–eosin (H&E), which is the primary staining method in medical diagnosis.[50] Hematoxylin was used to color nuclei of cells in blue followed by eosin to counterstain cytoplasm in red. Compared with the control group (**Figure 4**a), which did not have device implantations, the experimental group revealed no significant differences in terms of surgical pathology on one day (Figure 4b) and 7 days (Figure 4c) after implantation. As shown in Figure 4d, quantification of inflammation was expressed as the percentage of the stained nuclei area compared with the examined total area. The infiltration of inflammatory cells was only slightly increased on one day after implantation compared with the control group (1.88 ± 0.20% vs 1.36 ± 0.33%). There was also little difference in levels of infiltration of inflammatory cells 7 days after surgery (1.99 ± 0.31%), indicating that implantation of the single-crystalline generator had little inflammatory reaction. Consequently, the excellent biocompatibility based on histological analysis as well as a cell viability test implies the possibility of applying the flexible energy harvester to biomedical applications. We are currently developing chronologically biochemical and clinical investigations to inspect long-term biocompatibility of the implanted PMN-PZT-Mn device.

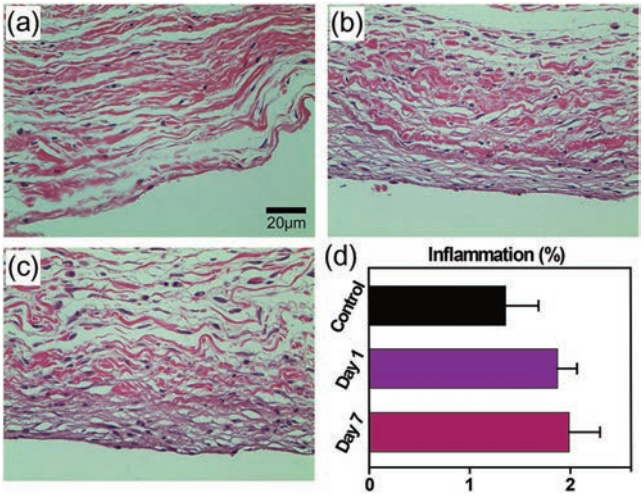


**Figure 4.** Histology images of a) control group, b) a day after, and c) 7 days after the implantation of the flexible energy harvester in the dorsal skin of a rat. d) Quantification of the percentage of inflammatory and fibrotic areas in the histological sections.

**Figure 5**a illustrates the experimental schematics of the self-powered wireless data transmission using the in vivo energy harvesting approach. The energy produced by cardiac motions was stored to a 22 μF capacitor through a full-wave bridge rectifier. When power supply pins of the transmitting part were connected to the capacitor that was charged enough to operate wireless communication, written data was wirelessly transmitted to the receiver using a communication protocol named wireless universal serial bus. To visually verify the wireless data transmission, the data was written as the instruction of switching on and off a light bulb at a long distance of about 5 m away.

Figure 5b shows circuit diagrams and photographs of the wireless communication module composed of the transmitting and receiving parts.[51] The voltage of the capacitor charged by the single-crystalline energy harvester was used to the drain voltage ($V_{DD}$) of the transmitting part (Figure 5b-i). When the drain voltage was supplied, the microcontroller unit (MCU) began to encode communication data. The total data size was 38 bytes long, which was composed of 2 bytes for the preamble, 32 bytes for the address, and 4 bytes for the message. The encoded data was sent to the transmitter from the MCU and then wirelessly transmitted to the receiving part in the form of radio frequency (RF) signals through an antenna. When the receiving part received the data, the receiver converted the RF signals to digital signals (Figure 5b-ii). The data was decoded through a decoder and then sent to a target application which was used to switch on and off the light bulb. To successfully operate wireless communication with a relatively small amount of energy generated by biomechanical movements, as shown in Figure 5c, analyzing the specifications of the communication module needs to be conducted. Figure 5c-i presents the voltage change of $V_{DD}$ triggered by wireless communication of which the steep slope in time from 29.8 to 34 ms indicates that the data was wirelessly transmitted. Operation of the communication module required a threshold voltage of above 2.3 V, therefore, the voltage drop after 34 ms resulted from a voltage beyond its inherent range of input voltage. Energy consumption for the wireless transmission was about 40.8 μJ as the voltage of a charged capacitor changed from 3.0 to 2.3 V (see the calculation in the Supporting Information). Figure 5c-ii shows the amount of current supplied to the module during wireless communication at a time scale magnified from 29 to 35 ms. The actual transmission occurred in 0.4 ms from the start-up and serial peripheral interface (SPI) process, preworks of the

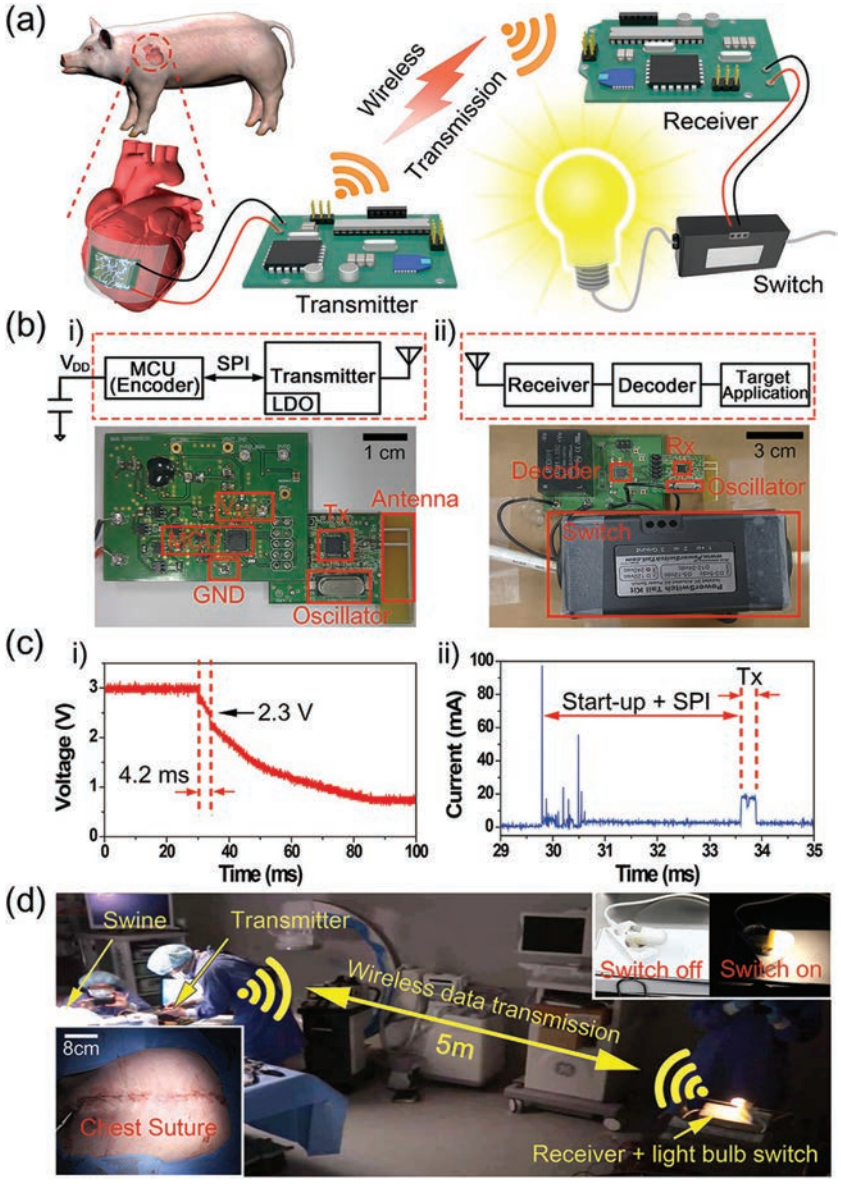


**Figure 5.** a) Experimental schematics of the self-powered wireless data transmission using biomechanical energy. The flexible energy harvester attached to porcine heart generates electricity from cardiac contraction and relaxation motions. The energy derived from cardiac motion was stored in the capacitor, and then the appointed data was transmitted to receiver wirelessly. A light bulb was repeatedly turned on and off as the data was used for the instruction of switching on and off the light bulb to visually verify data transmission. b) Circuit diagrams and photographs of the wireless communication module comprised of i) transmitting part and ii) receiving part. c) Specification of the wireless communication module. d) A photograph of the large animal model experiment. The left inset shows chest closure after the flexible energy harvester was implanted. The right inset shows the light bulb switched on and off with wireless data communication using biomechanical energy.

data transmission, took 3.8 ms. The total amount of charges for transmission, corresponding to the area under the curve, was easily calculated by integrating the current graph. Because the sharp peaks during the start-up and SPI process can be ignored due to its short generation time, the current of transmission (18 mA for 0.4 ms) mainly affected the total amount of charge. It is notable that based on a rough calculation, only a few microcoulomb were needed to transmit the data and then the single-crystalline energy harvester was capable of generating the amount of charge with in vivo energy harvesting.

Figure 5d shows the large animal experiment with a median sternotomy of a pig for in vivo energy harvesting. The flexible energy harvester was affixed to the porcine heart and worked stably even after chest closure, as shown in the left inset of Figure 5d. A 22 μF capacitor was connected to the device in parallel by a wire protruding the chest wall, and then the transmitter (CY3668 WirelessUSB NL Development Kit, Cypress Semiconductor Corporation) was connected to the capacitor again in parallel. The light bulb at a long distance from the transmitter was repeatedly switched on and off without any other power sources whenever the electricity charged in the capacitor was above the driving threshold voltage (as shown in Video S2 in the Supporting Information). It proves that wireless data transmission was successfully performed by biomechanical energy.

## 3. Conclusion

In conclusion, we have demonstrated practical usage of a high-performance single-crystalline flexible energy harvester by operating wireless data transmission with the electrical energy converted from heartbeats in a large animal model. The flexible energy harvester was sutured onto the epicardium after a median sternotomy. The energy harvester generated output voltage of 17.8 V and current of 1.75 μA from rhythmical porcine heartbeats, which were greater by a factor of 4.45 and 17.5 than that of previously reported in vivo piezoelectric energy harvesting. The electrical output, especially the output current, was well synchronized with the porcine ECG, which showed that the output was originally obtained from cardiac motion. Due to its accurate coincidence with the ECG signals, the energy harvester could also be applied to a heart monitoring sensor. The biocompatibility of the device was proved by a cell viability test and histological analysis. The cell viability test revealed no significant sign of cytotoxicity for various cells of three different species. Moreover, histology aspects showed that implantation of the single-crystalline device had little inflammatory reaction. Finally, the energy derived from porcine heartbeats was successfully used to wirelessly switch on and off a light bulb as practical application to a u-Health system.

## 4. Experimental Section

*Fabrication of the Flexible PMN-PZT-Mn Energy Harvester*: The single-crystalline PMN-PZT-Mn bulk block was grown by a solid-state crystal growth method and the composition was 0.4 $Pb(Mn_{0.33}Nb_{0.67})O_3$ – 0.6 $Pb(Zr_{0.42}Ti_{0.58})O_3$ with 0.5 mol% Mn doping. The PMN-PZT-Mn bulk block was bonded on a glass substrate with an adhesive wax that had a melting point of 60 °C. The PMN-PZT-Mn bulk was polished to a thin film with a thickness of 20 µm. The PMN-PZT-Mn thin film (2 cm × 3 cm × 20 µm) was fixed on a PET (3.5 cm × 7 cm × 75 µm) substrate that was coated with an adhesive epoxy (ultraviolet sensitive polyurethane). To separate the glass substrate from the PMN-PZT-Mn thin film, the sample was heated on a hotplate at the melting point of the adhesive wax for a few minutes. The Au interdigitated electrodes (IDEs, 100 nm thick) were deposited on the successfully transferred PMN-PZT-Mn thin film on a PET substrate. Encapsulation was performed with SU-8 passivation epoxy (2 µm in thickness) and then Cu electrical wires were connected to the Au IDE by silver paste. Finally, a poling process was carried out to align the dipoles by applying an electric field of 5 kV $mm^{-1}$ at room temperature for 3 h.

*In Vivo Study*: The investigation conformed to the Guide for the Care and Use of Laboratory Animals published by the US National Institutes of Health (NIH Publication, 8th edition, 2011). The study protocol was approved by the Institutional Animal Care and Committee of Yonsei University College of Medicine and Cardiovascular Research Institute (approval reference no. 2015-0220), and conformed to the guidelines of the American Heart Association. An adult Yorkshire pig (male, 40 kg) was anesthetized by intramuscular injection of ketamine (8 mg $kg^{-1}$) followed by intravenous propofol (1 mg $kg^{-1}$) injection, and then endotracheal intubation in the pig was performed for mechanical ventilation at a rate of 12 cycles per minute. Anesthesia was continued with the isoflurane dose fixed at 1.0%. After a median sternotomy, the energy harvester was sutured onto the epicardium with one stitch at each corner of the device. Cu wires attached to metal electrodes of the energy harvester were connected to a source-meter (Keithley 2612A) to measure the electrical output voltage and the current from cardiac contraction and relaxation motion.

*Cell Culture*: Human embryonic kidney (HEK293) cells were cultured in Dulbecco's modified Eagle's medium (DMEM; Gibco, Gaithersburg, MD, USA) supplemented with 10% heat-inactivated fetal bovine serum (FBS), 4-(2-hydroxyethyl)piperazine-1-ethanesulfonic acid, N-(2-hydroxyethyl)piperazine-N′-(2-ethanesulfonic acid) (HEPES, pH 7.4, $10 \times 10^{-3}$ M), 1% nonessential amino acids, penicillin (100 U $mL^{-1}$), and streptomycin (100 µg $mL^{-1}$). H9C2 embryonic rat heart-derived cells from ATCC were cultured in Dulbecco's modified Eagle's medium, supplemented with 10% FBS under 95% air/5% $CO_2$, and subcultured when at 50%–60% confluence. HL-1 cells from ATCC with cardiac phenotype were grown in fibronectin–gelatin coated flasks containing Claycomb medium (Sigma-Aldrich) and supplemented with 10% FBS, penicillin (100 U $mL^{-1}$), streptomycin (100 µg $mL^{-1}$), L-glutamine ($2 \times 10^{-3}$ M) and norepinephrine ($0.1 \times 10^{-3}$ M). Cells were cultured at 37 °C and 5% $CO_2$.

*Cell Viability Test*: Cells of control groups and those of experimental groups were grown on a general cell culture dish and a flexible energy harvester, respectively. The cultured cells were fixed with 4% ice cold formaldehyde (pH 7.2–7.3) for an hour at room temperature, then washed with phosphate-buffered saline (PBS) and permeated with 0.3% Triton X-100 for 30 min. The cells were washed and blocked with 5% bovine serum albumin (BSA) with 0.3% Triton X-100 in PBS for 30 min. The cells were washed and stained with $\alpha$-SMA as the first antibody using 1% BSA with 0.3% Triton X-100 in PBS through the night at cold room of 4 °C. The cells were washed and stained with Alexa Fluor 488 dye as the second antibody using 1% BSA with 0.3% Triton X-100 in PBS for 3 h at room temperature. Then, they were washed for 5 min and repeatedly washed three times, then stained with DAPI during the final washing. Fluorescence images were taken using a Zeiss LSM 710 confocal microscope (Carl Zeiss, Oberkochen, Germany).

*Histological Evaluation of In Vivo Biocompatibility*: The PMN-PZT-Mn flexible energy harvester with the size of 1 cm × 1 cm was inserted under the dorsal skin of randomly selected rats. The dorsal tissue was transversely sliced and fixed in 10% formalin, embedded in paraffin, and stained with H&E, which is the primary staining method in medical diagnosis. Quantification of inflammation and fibrotic area was expressed as the percentage of stained area in comparison with the total area of fields examined, using ImageJ, image analysis software (National Institutes of Health, Bethesda, MD, USA).

## Supporting Information

Supporting Information is available from the Wiley Online Library or from the author.

## Acknowledgements

D.H.K., H.J.S., and H.L. contributed equally to this work. This work was supported by research grants from the Korean Healthcare Technology R&D Project funded by the Ministry of Health & Welfare (Grant Nos. HI16C0058 and HI15C1200), and the by Nano Material Technology Development Program through the National Research Foundation of Korea (NRF) funded by the Ministry of Science, ICT and Future Planning (MSIP) (Grant No. 2016M3A7B4910636). This was also supported by the Global Frontier R&D Program on Center for Integrated Smart Sensors (Grant No. CISS-2016M3A6A6929958) funded by the MSIP through NRF of Korea government, and by the Wearable Platform Materials Technology Center (WMC) funded by the NRF Grant of the Korean Government (MSIP) (Grant No. 2016R1A5A1009926).

## Conflict of Interest

The authors declare no conflict of interest.

## Keywords

in vivo energy harvesting, piezoelectric single crystals, self-powered systems, wireless data transmission

Received: January 19, 2017
Revised: March 21, 2017
Published online: May 11, 2017

[1] H. J. Lee, S. H. Lee, K. S. Ha, H. C. Jang, W. Y. Chung, J. Y. Kim, Y. S. Chang, D. H. Yoo, *Int. J. Med. Inf.* **2009**, *78*, 193.
[2] N. Agoulmine, M. J. Deen, J.-S. Lee, M. Meyyappan, *IEEE Nanotechnol. Mag.* **2011**, *5*, 6.
[3] D. Panescu, *IEEE Eng. Med. Biol. Mag.* **2008**, *27*, 96.
[4] T. F. Budinger, *Annu. Rev. Biomed. Eng.* **2003**, *5*, 383.
[5] A. Yakovlev, S. Kim, A. Poon, *IEEE Commun. Mag.* **2012**, *50*, 152.
[6] L. Schwiebert, S. K. S. Gupta, J. Weinmann, in *Proc. 7th Annual Int. Conf. on Mobile Computing and Networking*, ACM, New York **2001**, pp. 151.
[7] M. A. Wood, K. A. Ellenbogen, *Circulation* **2002**, *105*, 2136.
[8] M. J. Wilhelm, C. Schmid, D. Hammel, S. Kerber, H. M. Loick, M. Herrmann, H. H. Scheld, *Ann. Thorac. Surg.* **1997**, *64*, 1707.
[9] H. Jang, H. Ma, K. Na, F. Bien, in *RF and Wireless Technologies for Biomedical and Healthcare Applications (IMWS-BIO 2015)*, IEEE, New York **2015**, pp. 101–102.

 

[10] P. Si, A. P. Hu, J. W. Hsu, M. Chiang, Y. Wang, S. Malpas, D. Budgett, in *2007 2nd IEEE Conf. Industrial Electronics and Applications*, IEEE, New York **2007**, pp. 235–239.
[11] R. H. Kim, H. Tao, T. Il Kim, Y. Zhang, S. Kim, B. Panilaitis, M. Yang, D. H. Kim, Y. H. Jung, B. H. Kim, Y. Li, Y. Huang, F. G. Omenetto, J. A. Rogers, *Small* **2012**, *8*, 2812.
[12] M. Song, M. Cheng, M. Xiao, L. Zhang, G. Ju, F. Shi, *Adv. Mater.* **2017**, *29*, 1603312.
[13] K. Song, J. H. Han, T. Lim, N. Kim, S. Shin, J. Kim, H. Choo, S. Jeong, Y. C. Kim, Z. L. Wang, J. Lee, *Adv. Healthcare Mater.* **2016**, *5*, 1572.
[14] A. Zurbuchen, A. Pfenniger, A. Stahel, C. T. Stoeck, S. Vandenberghe, V. M. Koch, R. Vogel, *Ann. Biomed. Eng.* **2013**, *41*, 131.
[15] A. Pfenniger, M. Jonsson, A. Zurbuchen, V. M. Koch, R. Vogel, *Ann. Biomed. Eng.* **2013**, *41*, 2248.
[16] Q. Zheng, B. Shi, F. Fan, X. Wang, L. Yan, W. Yuan, S. Wang, H. Liu, Z. Li, Z. L. Wang, *Adv. Mater.* **2014**, *26*, 5851.
[17] Q. Zheng, H. Zhang, B. Shi, X. Xue, Z. Liu, Y. Jin, Y. Ma, Y. Zou, X. Wang, Z. An, W. Tang, W. Zhang, F. Yang, Y. Liu, X. Lang, Z. Xu, Z. Li, Z. L. Wang, *ACS Nano* **2016**, *10*, 6510.
[18] Y. Ma, Q. Zheng, Y. Liu, B. Shi, X. Xue, W. Ji, Z. Liu, Y. Jin, Y. Zou, Z. An, W. Zhang, X. Wang, W. Jiang, Z. Xu, Z. L. Wang, Z. Li, H. Zhang, *Nano Lett.* **2016**, *16*, 6042.
[19] C. K. Jeong, K. M. Baek, S. Niu, T. W. Nam, Y. H. Hur, D. Y. Park, G. T. Hwang, M. Byun, Z. L. Wang, Y. S. Jung, K. J. Lee, *Nano Lett.* **2014**, *14*, 7031.
[20] Z. Li, G. Zhu, R. Yang, A. C. Wang, Z. L. Wang, *Adv. Mater.* **2010**, *22*, 2534.
[21] X. Cheng, X. Xue, Y. Ma, M. Han, W. Zhang, Z. Xu, H. Zhang, H. Zhang, *Nano Energy* **2016**, *22*, 453.
[22] Y. Yu, H. Sun, H. Orbay, F. Chen, C. G. England, W. Cai, X. Wang, *Nano Energy* **2016**, *27*, 275.
[23] C. Dagdeviren, Y. Shi, P. Joe, R. Ghaffari, G. Balooch, K. Usgaonkar, O. Gur, P. L. Tran, J. R. Crosby, M. Meyer, Y. Su, R. Chad Webb, A. S. Tedesco, M. J. Slepian, Y. Huang, J. A. Rogers, *Nat. Mater.* **2015**, *14*, 728.
[24] C. K. Jeong, S. B. Cho, J. H. Han, D. Y. Park, S. Yang, K. Il Park, J. Ryu, H. Sohn, Y. C. Chung, K. J. Lee, *Nano Res.* **2016**, *10*, 437.
[25] C. Sun, J. Shi, D. J. Bayerl, X. Wang, *Energy Environ. Sci.* **2011**, *4*, 4508.
[26] H. S. Lee, J. Chung, G. T. Hwang, C. K. Jeong, Y. Jung, J. H. Kwak, H. Kang, M. Byun, W. D. Kim, S. Hur, S. H. Oh, K. J. Lee, *Adv. Funct. Mater.* **2014**, *24*, 6914.
[27] G. T. Hwang, M. Byun, C. K. Jeong, K. J. Lee, *Adv. Healthcare Mater.* **2015**, *4*, 646.
[28] C. Dagdeviren, B. D. Yang, Y. Su, P. L. Tran, P. Joe, E. Anderson, J. Xia, V. Doraiswamy, B. Dehdashti, X. Feng, B. Lu, R. Poston, Z. Khalpey, R. Ghaffari, Y. Huang, M. J. Slepian, J. A. Rogers, *Proc. Natl. Acad. Sci. USA* **2014**, *111*, 1927.
[29] H. Zhang, X.-S. Zhang, X. Cheng, Y. Liu, M. Han, X. Xue, S. Wang, F. Yang, A. S. Smitha, H. Zhang, Z. Xu, *Nano Energy* **2015**, *12*, 296.
[30] G. T. Hwang, H. Park, J. H. Lee, S. Oh, K. Il Park, M. Byun, H. Park, G. Ahn, C. K. Jeong, K. No, H. Kwon, S. G. Lee, B. Joung, K. J. Lee, *Adv. Mater.* **2014**, *26*, 4880.
[31] J. H. Park, G. T. Hwang, S. Kim, J. Seo, H. Park, K. Yu, T. Kim, K. J. Lee, *Adv. Mater.* **2016**, *29*, 1603473.
[32] G. T. Hwang, J. Yang, S. H. Yang, H. Y. Lee, M. Lee, D. Y. Park, J. H. Han, S. J. Lee, C. K. Jeong, J. Kim, K. Il Park, K. J. Lee, *Adv. Energy Mater.* **2015**, *5*, 1500051.
[33] G.-T. Hwang, Y. Kim, J.-H. Lee, S. Oh, C. K. Jeong, D. Y. Park, J. Ryu, H. Kwon, S.-G. Lee, B. Joung, D. Kim, K. J. Lee, *Energy Environ. Sci.* **2015**, *8*, 2677.
[34] V. Annapureddy, M. Kim, H. Palneedi, H. Lee, S.-Y. Choi, W. Yoon, D. Park, J. Choi, B. Hahn, C. Ahn, J. Kim, D. Jeong, J. Ryu, *Adv. Energy Mater.* **2016**, *6*, 1601244.
[35] M. Ghamari, H. Arora, R. S. Sherratt, W. Harwin, in *2015 Int. Conf. on Computer Communications, and Control Technology (I4CT)*, IEEE, New York **2015**, pp. 1–6.
[36] J. Walk, T. Ussmueller, R. Weigel, G. Fischer, in *2011 IEEE Radio and Wireless Symp.*, IEEE, New York **2011**, pp. 406–409.
[37] T. Ativanichayaphong, S. J. Tang, L. C. Hsu, W. D. Huang, Y. S. Seo, H. F. Tibbals, S. Spechler, J. C. Chiao, in *2010 IEEE MTT-S Int. Microwave Symp. Dig. (MTT 2010)*, IEEE, New York **2010**, pp. 608–611.
[38] S. Zhang, S.-M. Lee, D.-H. Kim, H.-Y. Lee, T. R. Shrout, *Appl. Phys. Lett.* **2008**, *93*, 122908.
[39] O. Bilgen, M. Amin Karami, D. J. Inman, M. I. Friswell, *Smart Mater. Struct.* **2011**, *20*, 055024.
[40] B. Lu, Y. Chen, D. Ou, H. Chen, L. Diao, W. Zhang, J. Zheng, W. Ma, L. Sun, X. Feng, *Sci. Rep.* **2015**, *5*, 16065.
[41] K. F. Tan, K. L. Chan, K. Choi, in *2000 First Int. Conf. Advances in Medical Signal and Information Processing (IEE Conf. Publ. No. 476)*, IET, New York **2000**, pp. 41–47.
[42] A. Zomorrodian, N. J. Wu, S. Wilczac, C. Colbert, A. Ignatiev, in *Proc. of the 13th IEEE Int. Symp. on Applications of Ferroelectronics*, IEEE International Symposium on Applications of Ferroelectrics, New York **2002**, pp. 129–132.
[43] J. Tian, P. Han, J. F. Carroll, D. A. Payne, in *IEEE International Ultrasonics Symposium (IUS)*, IEEE, New York **2009**, pp. 972–975.
[44] A. A. Heitmann, J. A. Stace, L. C. Lim, A. H. Amin, *J. Appl. Phys.* **2016**, *119*, 224101.
[45] K. V. Nemani, K. L. Moodie, J. B. Brennick, A. Su, B. Gimi, *Mater. Sci. Eng. C* **2013**, *33*, 4453.
[46] S. H. Cho, H. M. Lu, L. Cauller, M. I. Romero-Ortega, J. B. Lee, G. A. Hughes, *IEEE Sens. J.* **2008**, *8*, 1830.
[47] J. D. Williams, W. Wang, *Microsyst. Technol.* **2004**, *10*, 699.
[48] Y. Zhang, X. Zhang, J. Fang, S. Jiang, Y. Zhang, D. Gu, R. D. Nelson, J. C. LaRue, in *2010 5th IEEE Int. Conf. on Nano/Micro Engineered and Molecular Systems*, IEEE, New York **2010**, pp. 395–398.
[49] S. Tuomikosky, S. Franssila, *Phys. Scr.* **2004**, *T114*, 223.
[50] H. Park, H. Park, D. Lee, S. Oh, J. Lim, H. J. Hwang, S. Park, H. N. Pak, M. H. Lee, B. Joung, *Circ. J.* **2014**, *78*, 2292.
[51] Cypress Semiconductor Corporation—CY3668 WirelessUSB NL Development Kit, http://www.cypress.com/documentation/development-kitsboards/cy3668-wirelessusb-nl-development-kit (accessed: March 2013).